

First-Principles Study of Charged Point Defects in 4H-SiC: Accurate Formation Energies, Trap Levels, and Beyond

Haruhide Miyagi
EDAG

Nihon Synopsys G.K.
Tokyo, Japan

Haruhide.Miyagi@synopsys.com

Ulrik G. Vej-Hansen
EDAG

Synopsys Denmark ApS
Copenhagen, Denmark

Ulrik.Vej-Hansen@synopsys.com

Brad A. Wells
EDAG

Synopsys Denmark ApS
Copenhagen, Denmark

Bradley.Wells@synopsys.com

Jan-Niclas Luy
EDAG

Synopsys Denmark ApS
Copenhagen, Denmark

Jan-Niclas.Luy@synopsys.com

Christoph Zechner
EDAG

Synopsys GmbH
Aschheim/Dornach, Germany

Christoph.Zechner@synopsys.com

Abstract—To accurately investigate the properties of charged defects in 4H-SiC, large-scale *ab initio* simulations are carried out with the QuantumATK atomic-scale modeling platform by Synopsys. For a variety of charged defects, calculations of formation energies and trap levels are performed using density functional theory with the hybrid HSE06 XC-functional and linear combination of atomic orbitals basis sets. Agreement of the computed trap levels of carbon vacancies with experimentally observed levels validates the accuracy and reliability of the simulation. With the nudged elastic band method, diffusion properties are also computed and analyzed. Finally, by calculating the phonon density of states in each system using a moment tensor potential trained for 4H-SiC, the vibrational correction is made to obtain the equilibrium concentration of each charged defect at finite temperatures.

Keywords—4H-SiC, charged defects, formation energies, trap levels, diffusion barriers, equilibrium concentrations, diffusivities, density functional theory (DFT), hybrid functionals, HSE06, nudged elastic band (NEB), moment tensor potentials (MTPs), process model calibration.

I. INTRODUCTION

Silicon carbide polytype 4H (4H-SiC) is widely considered for power electronics because of its excellent physical properties (see, e.g., [1]). Point defects play an important role in 4H-SiC device manufacturing steps, such as implantation and annealing. Interstitials and vacancies facilitate dopant diffusion, the formation of larger defects and may impact dopant activation. Moreover, point defects may occur in several charge states. Trap levels act as recombination centers in the bandgap and degrade device performance. An accurate knowledge of charged point defect properties in 4H-SiC is important for the understanding and modeling of device fabrication processes and electrical device characteristics.

Recently, a process model has been developed for carbon vacancies (V_C) and model parameters have been calibrated [2] against corresponding defect profiles measured with deep-level transient spectroscopy (DLTS). For other native point defects in 4H-SiC, a similar extraction of properties from measurements is hindered by a lack of suitable data. First-principles calculations are needed to establish good values for trap levels, equilibrium concentrations and diffusivities. This work aims at accurately calculating the formation energies, trap levels, and diffusion barriers for a variety of charged defects with density functional theory (DFT).

The calculation of prefactors of point defect equilibrium concentrations and diffusivities requires a computation of the

phonon density of states (DOS) which is numerically intractable with first-principles methods for these systems. This work demonstrates how to overcome this numerical difficulty by using moment tensor potentials (MTP) [3], a machine-learned forcefield. Present preliminary results of equilibrium concentrations are also shown.

II. MODELING AND SIMULATION METHOD

Bulk 4H-SiC containing a charged defect was modeled by a $4 \times 4 \times 2$ supercell of 4H-SiC consisting of 256 atoms, in which each of the following defects was created: V_C , silicon vacancies (V_{Si}), silicon substitutionals to carbon (Si_C), carbon substitutionals to silicon (C_{Si}), carbon interstitials (C_i), silicon interstitials (Si_i), carbon vacancy-antisite pairs (V_C-C_{Si}), and silicon vacancy-antisite pairs ($V_{Si}-Si_C$). Figure 1 represents a defect of type $V_C^q(h)$, i.e., a carbon vacancy with charge q ($= -2, -1, 0, 1, 2$) at h site.

Calculations of defect formation energies, concentrations, and diffusion barriers were performed with DFT using the hybrid HSE06 XC-functional and linear combination of atomic orbitals (LCAO) basis sets [4, 5], implemented in the QuantumATK atomic-scale modeling platform by Synopsys

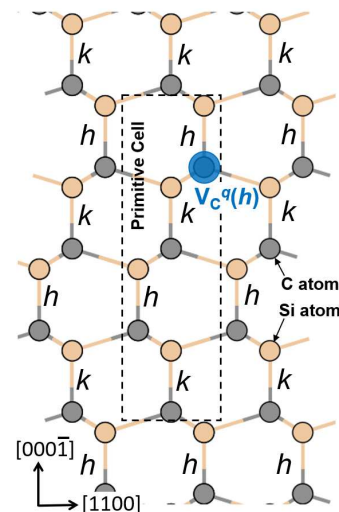


Figure 1: Schematic representation of creating $V_C^q(h)$, i.e., a carbon vacancy with charge q ($= -2, -1, 0, 1, 2$) at h site in 4H-SiC; note that there are two inequivalent lattice sites, i.e., h and k sites, as indicated in the figure. The dashed box indicates the 8-atom primitive unit cell containing four silicon (carbon) atoms colored in yellow (gray). In this example, a carbon atom at h site is replaced by a ghost atom with adding the charge q . The removed carbon atom is added to bulk diamond, whereas the charge q comes from an electron reservoir, the electron chemical potential of which is defined with respect to the top of the valence band.

[6, 7]. In this work the mixing parameter in HSE06 was set to be 0.263, which reproduces the experimental bandgap 3.23 eV of 4H-SiC at $T=300$ K [8]. To estimate the phonon DOS of each defect, additional calculations were carried out using a forcefield MTP trained for 4H-SiC neutral defects using the PBE DFT functional.

In each system the atomic positions were fully relaxed with DFT using HSE06/LCAO. The formation energy of the charged defect was computed with bulk silicon and diamond used for atomic reference energies. Finite size corrections were also added for charged states [9]. For calculation of vacancy formation energies, removed atoms were replaced with a ghost atom, to correct for the basis set superposition error. The trap levels were then obtained as the energy to transition between charge states. Calculations with the climbing-image nudged elastic band (CI-NEB) method [10] were also carried out to obtain the migration diffusion barriers. For defects and transition states the phonon DOS was used to estimate the entropy and free energy based on the quasi-harmonic approximation [11]. This simulation process is hereafter called vibrational correction to obtain equilibrium concentrations and diffusivities at finite temperatures. Because MTPs estimate the energy and forces by interpolating between training structures the quality of the potential depends on the training set and can be improved by expanding this training set.

See Fig. 2 which summarizes the workflow and illustrates how MTPs make the vibrational correction numerically feasible and potentially also accelerate relaxation for formation energy calculations and NEB simulations.

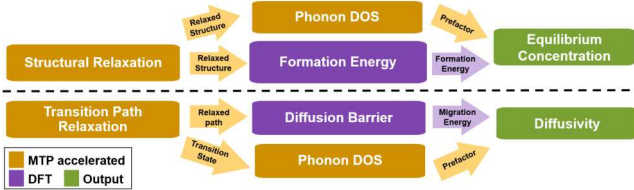


Figure 2: Simulation workflow in this project. Using moment tensor potentials (MTPs) makes calculation of the phonon density of states (DOS), and consequentially equilibrium concentrations and diffusivities, numerically feasible. Using MTPs in pre-relaxation could accelerate formation energy calculations and NEB simulations by reducing the number of steps required for relaxation with DFT. The blocks in gold indicate the parts of the simulation flow which MTPs can accelerate.

III. RESULTS AND DISCUSSION

Among the defects modeled in this work, carbon vacancies are commonly observed in all as-grown 4H-SiC; their trap levels have been experimentally studied in detail and identified as the $Z_{1/2}$ and $EH_{6/7}$ centers [1]. In this section some preliminary results of carbon vacancies and other defects are presented and compared with literature values to assess the simulation validity and to illustrate the physics behind the results.

A. Formation Energies and Trap Levels of Defects

Looking at the trap levels of V_C shown in Table 1 and Fig. 3 it can be noted that the calculated levels in this work and the experimental levels [12-14] are in good agreement up to the negative-U property of the levels. The trap levels after the vibrational correction are presented in parenthesis of Table 1, indicating the correction has only a minor effect on the trap levels. Table 1 also shows larger differences between the

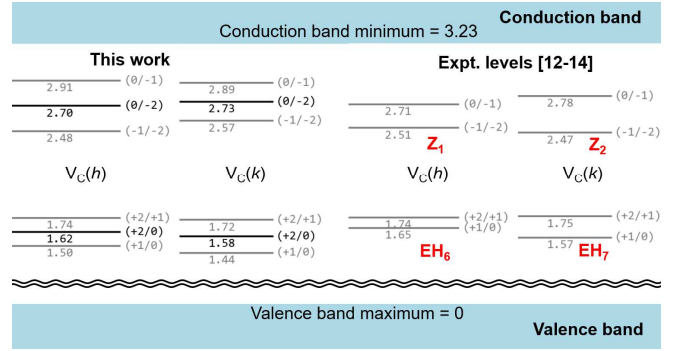


Figure 3: Plots of the trap levels of carbon vacancies in 4H-SiC: (left) results in this work without the vibration correction; (right) experimental levels [12-14]. The levels are measured relative to the valence band maximum and shown in units of eV. The levels colored in gray indicate the negative-U property (metastable states).

Defect	(+2/+1)	(+1/0)	(0/-1)	(-1/-2)	(+2/0)	(0/-2)
$V_C(h)$	1.74 (1.72)	1.50 (1.45)	2.91 (2.89)	2.48 (2.45)	1.62 (1.59)	2.70 (2.67)
$V_C(k)$	1.72 (1.69)	1.44 (1.39)	2.89 (2.88)	2.57 (2.53)	1.58 (1.54)	2.73 (2.70)
$V_C(h)$ [12-14]	1.74	1.65	2.71	2.51		
$V_C(k)$ [12-14]	1.75	1.57	2.78	2.47		
$V_C(h)$ [15]	1.64	1.84	2.71	2.79		
$V_C(k)$ [15]	1.67	1.75	2.80	2.74		2.77
$V_C(h)$ [16]	1.65	2.03	2.47			
$V_C(k)$ [16]	1.74	1.96	2.58	3.10		

Table 1: Trap levels of carbon vacancies in 4H-SiC. The levels are measured relative to the valence band maximum and shown in units of eV. The values in parentheses are the levels after the vibration correction. The experimental levels [12-14], and calculated levels [15, 16] are also listed for comparison. The levels colored in gray indicate the negative-U property (metastable states).

Defect	Formation energy (eV)
$V_C^{q=0}(h)$	4.94 (4.85)
$V_C^{q=0}(k)$	4.82 (4.72)
$V_C^{q=0}(h)$ [16]	4.88
$V_C^{q=0}(k)$ [16]	4.84

Table 2: Formation energies of neutral carbon vacancies in 4H-SiC. The values computed at the C-rich limit are shown in units of eV. The calculated values of the neutral states in [16] are also shown for comparison.

calculated levels reported in [15, 16] and the experimental levels. Turning to the formation energies listed in Table 2, the formation energies of the neutral states calculated in this work and those in [16] are in good agreement. These comparisons show the overall validity of our approach.

Note that the DFT simulations in [15] employed a $4 \times 4 \times 4$ supercell and used HSE06/PlaneWave (PW) in formation energy calculations but used PBE/PW in relaxation to reduce the numerical cost. Likewise, the DFT simulations in [16] used HSE06/PW in both relaxation and formation energy calculations but employed a $4 \times 4 \times 1$ supercell to reduce the cost. Based on these observations, reproducing the experimental levels hence requires a supercell greater than or

Defect	(+2/+1)	(+1/0)	(0/-1)	(-1/-2)	(+2/0)	(0/-2)
$V_{Si}(h)$	0.228	0.833	1.40	1.97		
$V_{Si}(k)$	0.148	0.752	1.32	1.88		
$C_{Si}(h)$	-0.0266	0.110	3.22	3.37		
$C_{Si}(k)$	0.0427	0.0428	3.20	3.36		
$Si_C(h)$	-0.153	0.272	3.28	3.57		
$Si_C(k)$	-0.150	0.271	3.29	3.57		
$V_C(h)-C_{Si}(h)$	1.60	2.19	2.53	2.76		
$V_C(h)-C_{Si}(k)$	1.64	2.20	2.45	2.94		
$V_C(k)-C_{Si}(h)$	1.60	2.14	2.48	2.96		
$V_C(k)-C_{Si}(k)$	1.73	2.23	2.48	2.70		
$V_{Si}(h)-Si_C(h)$	1.71	1.48	2.91	2.50	1.60	2.70
$V_{Si}(h)-Si_C(k)$	1.70	1.43	2.89	2.59	1.57	2.74
$V_{Si}(k)-Si_C(h)$	1.72	1.49	2.90	2.50	1.60	2.70
$V_{Si}(k)-Si_C(k)$	1.70	1.43	2.90	2.58	1.56	2.74

Table 3: Trap levels for silicon vacancies (V_{Si}), antisites (C_{Si} and Si_C), carbon vacancy-antisite pairs (V_C-C_{Si}), and silicon vacancy-antisite pairs ($V_{Si}-Si_C$). The levels are measured relative to the valence band maximum and in units of eV. The levels colored in gray indicate the negative-U property (metastable states), whereas the levels colored in blue indicate that they are located outside the bandgap. The levels of carbon interstitials and silicon interstitials are not shown due to the limitation of space.

equal to $4 \times 4 \times 2$ and HSE06 in both relaxation and formation energy calculations. This is numerically feasible in reasonable computational time when using HSE06/LCAO with which the numerical cost of computing the exchange matrix scales linearly with the number of k-points and system size N . Using HSE06/PW the computational cost scales as $O(N^3 \log(N))$ [17], making this method infeasible at large scale.

Calculated trap levels of other charged defects are shown in Table 3. Other than for V_C , these values cannot be compared to reliable experimental values. With the same methods used for calculation, a similar accuracy can be expected, though.

B. Equilibrium Concentrations of Defects

After obtaining the formation energy of each charged defect, the vibrational correction was calculated with force-field simulations using the MTP to obtain the equilibrium concentration at finite temperatures.

The equilibrium concentrations of neutral C_{Si} and Si_C , are plotted in Fig. 4 (a). These are summed over all atomic sites

for each defect type. Note that the concentration of C_{Si} is higher than that of Si_C . This is expected as it is easier to substitute a smaller-sized atom at the site of a larger-sized atom, making the formation energy of each charged state of C_{Si} smaller than Si_C . This observation indicates the validity of these simulations. With the vibrational correction, the difference becomes larger.

Figure 4 (b) plots the equilibrium concentrations of neutral V_C . Within one order of magnitude, the values, including the corrections for vibrational entropy, agree with the total concentrations of V_C reported in [2]. Those originate from fitting a process simulation model to DLTS profiles of $Z_{1/2}$ defects. Several reasons could account for the remaining mismatch. (i) The MTP used for calculation of vibrational corrections has been newly developed and may require further training. (ii) The HSE06 XC-functional, accurate only within 0.5 eV when benchmarked against known defect energies in Si [18], might not be perfectly accurate for defect formation energies in 4H-SiC, neither. Small inaccuracies in the formation energy impact equilibrium concentration results significantly, via a Boltzmann factor. (iii) When defining the formation energy of V_C , it is important where the removed C atom is added to. In our DFT simulations, C atoms are added to pristine diamond, which has a similar chemical potential for C atoms as graphite. In the experiments used in [2], SiC wafers were covered by C-cap layers, created by graphitized photoresist films. C atoms escaping 4H-SiC and leaving behind V_C 's ended up in the C-cap. The chemical potential of C in a C cap is probably close to the one in graphite, but not necessarily identical. (iv) The calculated $V_C^{q=0}$ concentrations shown in Fig. 4 (b) do not include charged states (i.e., $q \neq 0$).

C. Defect Migrations

Compared with the formation energies, calculations of diffusion barriers require significantly more computational resources for determining transition states. Likewise, calculations of diffusivities are computationally more demanding than calculations of equilibrium concentrations even when using MTPs. This section presents proof-of-concept results about diffusion barriers of some selected charged defects.

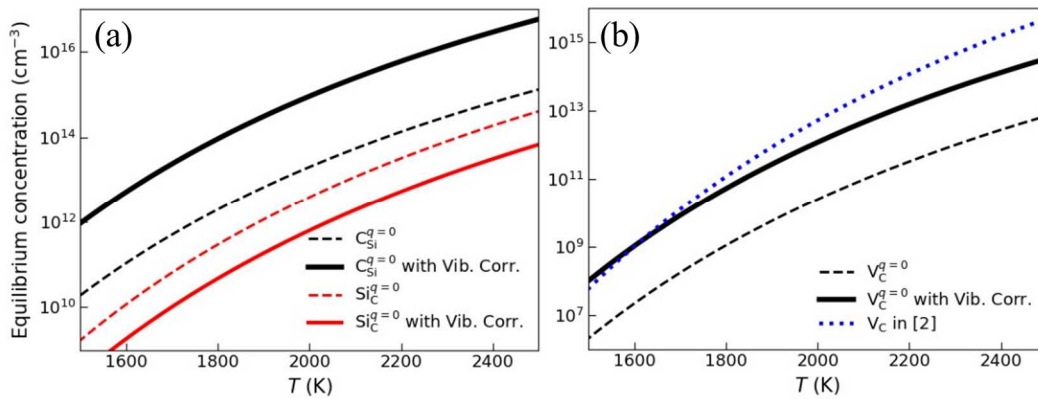


Figure 4: Plots of the equilibrium concentrations of (a) C_{Si} and Si_C , and (b) V_C in bulk 4H-SiC. Dashed (solid) lines represent the calculated concentrations of neutral charged states without (with) the vibrational correction. Note that these results were computed with the formation energies from the definition of the atomic chemical potentials as described in the main text; this definition corresponds to C-rich condition in the evaluations of V_C in (b). Dotted blue line in (b) shows the equilibrium concentrations of V_C at the 4H-SiC surface covered by a C cap layer, as reported in [2] based on process model calibration against DLTS profiles of V_C .

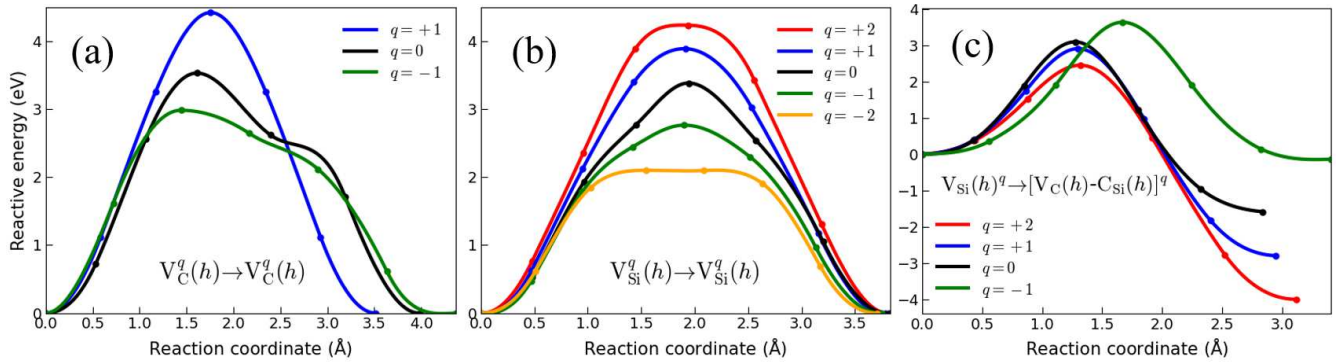


Figure 5: Plots of the energy barrier in defect migrations of (a) $V_C^q(h) \rightarrow V_C^q(h)$, (b) $V_{Si}^q(h) \rightarrow V_{Si}^q(h)$, and (c) $V_{Si}^q(h) \rightarrow [V_C(h) - C_{Si}(h)]^q$, computed with the nudged elastic band method. The energies are shown in units of eV and measured relative to the energy of the first image in each panel, i.e., the energy of $V_C^q(h)$ in (a), and the energy of $V_{Si}^q(h)$ in (b) and (c) without the vibrational correction. Note that these results were computed with the formation energies from the definition of the atomic chemical potentials as described in the main text.

Looking first at Figs. 5 (a) and (b) which, respectively, show the energy for defect migrations, $V_C^q(h) \rightarrow V_C^q(h)$ and $V_{Si}^q(h) \rightarrow V_{Si}^q(h)$, it can be seen in both cases that the diffusion barriers increase as the charge q increases. In the NEB simulations in [19], the same trend is observed for carbon vacancies and partly for silicon vacancies; there, the diffusion barrier of silicon vacancies increases as the charge goes from -2 to 0 and does not change significantly from 0 to +2 [19]. The difference is likely due to differences in the computational details between the studies.

Looking then at Fig. 5 (c) the results of $V_{Si}^q(h) \rightarrow [V_C(h) - C_{Si}(h)]^q$ are shown. Interestingly, in this case, the diffusion barrier decreases as the charge q increases. Hence, Fig. 6 (b) and (c) show that not only the diffusion barrier but also the diffusion path of $V_{Si}(h)$ highly depend on its charged state, indicating the possibility to control the diffusion of $V_{Si}(h)$ in annealing processes of 4H-SiC. However, more calculations, analysis, as well as careful accuracy assessments are needed for investigating the details of the defect migrations and clarifying the underlying physics.

IV. CONCLUDING REMARKS

For a variety of charged defects in 4H-SiC, calculations of formation energies and trap levels were performed with DFT using HSE06/LCAO. The computed trap levels of V_C agree well with experimentally observed levels, indicating a high reliability and accuracy of calculated defect trap levels. For C_{Si} , Si_C , and V_C , the equilibrium concentrations at finite temperatures have been computed by carrying out a vibrational correction, i.e., combining formation energies calculated with DFT and the vibrational entropy calculated with an MTP. For V_C , the obtained equilibrium concentration agrees to the values reported from experiments within a factor of 10. Finally, diffusion barriers of some selected charged defects were computed with the NEB method and presented.

The goal of this work is systematic and accurate calculations of formation energies, trap levels, equilibrium concentrations, and diffusivities of important defects in 4H-SiC. The results are planned to be used in the process model calibration of commercial TCAD software.

REFERENCES

- [1] T. Kimoto and J. A. Cooper, *Fundamentals of Silicon Carbide Technology* (John Wiley & Sons, Singapore, 2014).
- [2] C. Zechner, M. Tanaka, K. Shimai, N. Zographos, S. Kanie, and S. Tsuboi, *J. Appl. Phys.* **132**, 035702 (2022).
- [3] A. V. Shapeev, *Multiscale Model. Simul.* **14**, 1153 (2016).
- [4] J. Heyd et al., *J. Chem. Phys.* **124**, 219906 (2006).
- [5] S. V. Levchenko et al., *Comp. Phys. Comm.* **192**, 60 (2015).
- [6] QuantumATK U-2022.12, Synopsys QuantumATK (<https://www.synopsys.com/silicon/quantumatk.html>); this work used some new frameworks and features in engineering releases of QuantumATK V-2023.09.
- [7] S. Smidstrup, T. Markussen, P. Vancraeyveld, J. Wellendorff, J. Schneider, T. Gunst, B. Verstichel, D. Stradi, P. A. Khomyakov, U. G. Vej-Hansen, M.-E. Lee, S. T. Chill, F. Rasmussen, G. Penazzi, F. Corsetti, A. Ojanperä, K. Jensen, M. L.N. Palsgaard, U. Martinez, A. Blom, M. Brandbyge, K. Stokbro. *J. Phys.: Condes. Matter* **32**, 015901 (2020).
- [8] M. E. Levinshtein, S. L. Rumyantsev, and M. S. Shur, *Properties of Advanced Semiconductor Materials: GaN, AlN, InN, BN, SiC, SiGe* (John Wiley & Sons, Inc., New York, 2001) 93-148.
- [9] C. Freysoldt, J. Neugebauer, and C. G. Van de Walle, *Phys. Rev. Lett.* **102**, 016402 (2009).
- [10] G. Henkelman, B. P. Uberuga, and H. Jonsson, *J. Chem. Phys.* **113**, 9901 (2000).
- [11] M. T. Dove, *Introduction to lattice dynamics* (Cambridge University Press, Cambridge, 1993).
- [12] C. G. Hemmingsson, N. T. Son, A. Ellison, J. Zhang, and E. Janzén, *Phys. Rev. B* **58**, R10119 (1998).
- [13] C. G. Hemmingsson, N. T. Son, A. Ellison, J. Zhang, and E. Janzén, *Phys. Rev. B* **59**, 7768 (1999).
- [14] D. Booker, E. Janzén, N. T. Son, J. Hassan, P. Stenberg, and E. Ö. Sveinbjörnsson, *J. Appl. Phys.* **119**, 235703 (2016).
- [15] T. Hornos, A. Gali, and B. G. Svensson, *Mater. Sci. Forum* **679-680**, 261 (2011).
- [16] T. Kobayashi, K. Harada, Y. Kumagai, F. Oba, and Y. Matsushita, *J. Appl. Phys.* **125**, 125701 (2019).
- [17] P. A. Khomyakov, J. Wellendorff, M. Palsgaard, T. Gunst, H. Miyagi, B. Verstichel, F. Corsetti, V. Arcisauskaitė, U. Martinez, A. Blom, and S. Smidstrup, *Proc. of SISPAD 2021* (Dallas, TX, USA), pp. 124-127, Sep. 2021.
- [18] Y. Park, C. Zechner, Y. Oh, H. Kim, I. Martin-Bragado, E. M. Bazizi, and F. Benistant, 2017 IEEE International Electron Devices Meeting (IEDM), (San Francisco, CA, USA), pp. 35.3.1-35.3.4, Dec. 2017.
- [19] X. Yan, P. Li, L. Kang, S.-H. Wei, and B. Huang, *J. Appl. Phys.* **127**, 085702 (2020).